



A Ca-deficient hydroxyapatite (CDHA)/MgF₂ bi-layer coating with unique nano-scale topography on biodegradable high-purity Mg

Junlei Li^a, Wenwu Xu^a, Xiao Lin^b, Fang Cao^a, Jiahui Yang^a, Lu Li^a, Xiaowei Wei^a, Xiuzhi Zhang^a, Dewei Zhao^{a,*}, Ke Yang^c

^a Department of Orthopaedics, Affiliated Zhongshan Hospital of Dalian University, Dalian 116001, China

^b Orthopaedic Institute, Medical College, Soochow University, Suzhou, Jiangsu Province 215006, China

^c Institute of Metal Research, Chinese Academy of Sciences, Shenyang 110016, China

ARTICLE INFO

Keywords:

Biodegradable Mg
CDHA/MgF₂ bi-layer coating
Nanorod-like morphology
Corrosion resistance
Osteogenic capability

ABSTRACT

Enhanced corrosion resistance and accelerated new bone formation are desired to make Mg and its alloys to be ideal candidate for bone biomaterial. For this purpose, a CDHA/MgF₂ bi-layer coating was prepared on high purity Mg by a combination of fluoride treatment and hydrothermal treatment. The coating exhibited a nanoscale surface topography. Enhanced adhesion strength and corrosion resistance was obtained for the CDHA/MgF₂ bi-layer coating. In vitro cell experiment showed that the adhesion, proliferation and differentiation of MG63 cells were significantly improved on Mg with CDHA/MgF₂ coating compared to that on Mg with HA coating and MgF₂ coating. In conclusion, this study provides a promising surface modification method for Mg metal with enhanced corrosion resistance and superior osteogenic bioactivity.

1. Introduction

Magnesium and its alloys have been widely studied as biodegradable medical metallic biomaterials [1]. However, the degradation rate of most Mg-based metallic materials is far surpasses the bone healing rate, which tends to produce a gap at the interface between the Mg-based implants and their surrounding bone tissue [2,3]. Surface modification techniques, such as micro-arc oxidation (MAO) [4], electro-deposition [5,6], sol-gel method [7], biomimetic deposition [8], are reportedly effective to improve the corrosion resistance of Mg-based metallic materials. Besides suitable protective capability, good biocompatibility and osteogenic activity are also desired for the surface coatings on the Mg-based implants [9].

Among various surface modification techniques, fluoride treatment has been reported to be an effective candidate to improve the corrosion resistance of Mg [7]. MgF₂ coating exhibited high bonding strength and good biocompatibility [10]. However, there is no clear evidence indicating that the MgF₂ coating can improve osteogenesis. In many studies, MgF₂ coating was used as the interlayer and a bioactive coating was fabricated on MgF₂ coating to obtain a bi-layer or multilayer bi-layer coatings with enhanced corrosion resistance, good biocompatibility and bio-functionalization [10]. Calcium phosphate (CaP) coatings significantly decreased the degradation rate of the Mg-based

implants, and satisfactory biocompatibility and enhanced biological properties associated with osteogenesis were also observed for the Mg-based implants with CaP coatings [11]. Therefore, CaP coatings were widely studied as the outermost layer of the bi-layer coatings.

Among various CaP coating, Hydroxyapatite (HA, Ca₁₀(PO₄)₆(OH)₂), the major mineral component of bones, is widely used as surface coating of orthopedic implants. It has been proven that HA coating is beneficial to the adhesion, proliferation, differentiation of primary human osteoblast cells. The HA coating was also found to promote alkaline phosphatase activity of osteoblast cells [12]. In addition, degradation rate of HA in vivo was found to be slower than that of other calcium phosphate phases, so better protection to the Mg substrate could be obtained from the HA coating [13]. In this study, we first passivated the surface of Mg with hydrofluoric acid, and MgF₂ coating was obtained on the surface of Mg substrate. Then hydrothermal treatment was carried out to fabricate a HA/MgF₂ bi-layer coating in order to increase the corrosion resistance and osteogenic capability of Mg. The physicochemical properties and corrosion resistance of the HA/MgF₂ bi-layer coating were characterized. The biological performance of the HA/MgF₂ bi-layer coating was tested by in vitro cell experiments using human osteoblast-like MG63 cells to observe cell adhesion, proliferation and osteogenic differentiation potential.

* Corresponding author.

E-mail address: zhaodewei2016@163.com (D. Zhao).

<https://doi.org/10.1016/j.colsurfb.2020.110911>

Received 7 November 2019; Received in revised form 24 February 2020; Accepted 27 February 2020

Available online 27 February 2020

0927-7765/ © 2020 Elsevier B.V. All rights reserved.

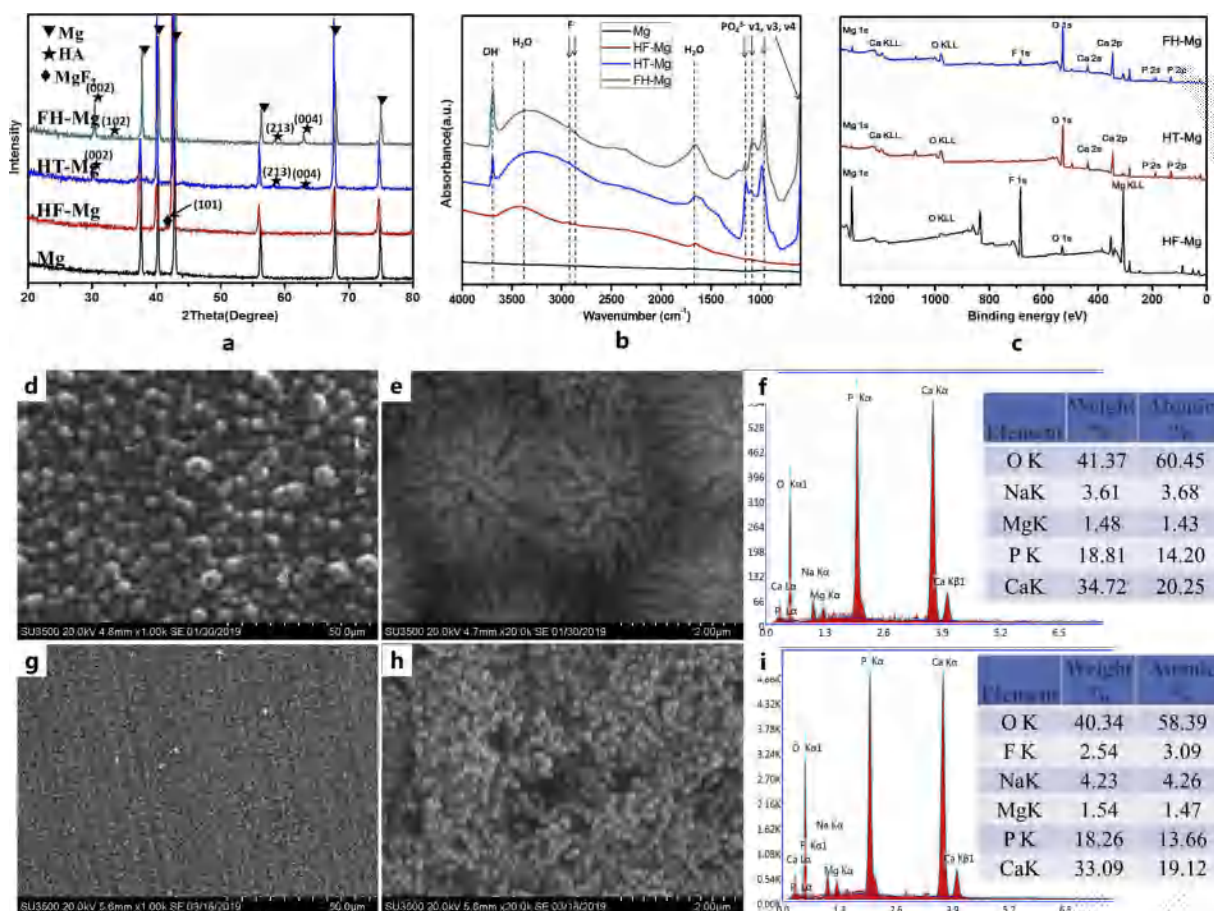


Fig. 1. (a) XRD patterns of Mg, HF-Mg, HT-Mg and FH-Mg; (b) FTIR spectra of Mg, HF-Mg, HT-Mg and FH-Mg; (c) XPS spectra of Mg, HF-Mg, HT-Mg and FH-Mg; the surface morphologies and element components of HT-Mg (d-f) and FH-Mg (g-i).

2. Results

2.1. Surface physicochemical properties

The XRD patterns of the Mg, HF-Mg, HT-Mg and FH-Mg are shown in Fig. 1a. The typical peaks of Mg can be observed in all of the XRD patterns. The peak at 41.1° corresponding to sellaite (MgF_2) could be observed in the HF-Mg, indicating the formation of fluoride layer. In the pattern of HT-Mg and FH-Mg, significant HA peaks were detected. Fig. 1b shows the FTIR spectra of Mg, HF-Mg, HT-Mg and FH-Mg. HF-Mg, HT-Mg and FH-Mg show absorption peaks at 1643 cm^{-1} and 3375 cm^{-1} , which are attributed to the adsorbed water molecules. The absorption peaks at 2928 and 2857 cm^{-1} of HF-Mg and FH-Mg were due to the presence of the F^- ion, indicating the existence of fluoride layer. Absorbance peak at about 3695 cm^{-1} was due to the presence of OH⁻ ion, the characteristic peak of HA. The absorptions at 1145 , 1074 , 964 and 600 cm^{-1} can be attributed to the PO_4^{3-} group. As shown in Fig. 1c, XPS analysis was also carried out to characterize the coatings. The surface of HF-Mg is mainly composed of Mg and F, indicating the formation of the a MgF_2 coating. The surface of HT-Mg is composed of Ca, O, P, Na and Mg. Two major peaks of Ca 2p (347.1 eV and 351.2 eV) and only one peak of P 2p (132.9 eV) correspond to Ca and P groups in crystalline HA. The existence of Na 1s (1071.6 eV) and Mg 1s (1303.3 eV) indicated that Na and Mg substituted the position of Ca. As for FH-Mg, element F was also detected besides Ca, O, P, Na and Mg.

As shown in Fig. 1d, the surface of the HT-Mg appears to be rugged with cracks observed, and clusters with different sizes are visible. At $20,000\times$ magnification Fig. 1e), the clusters showed nanoneedle-like

morphology. The EDS in Fig. 1f showed that the coating contained Ca, P, Mg, Na and O. The Mg^{2+} and Na^+ ions might substitute the Ca^{2+} position. The Ca/P ratio was about 1.43, which was lower than the stoichiometric value in HA (1.67), indicating that the Ca-deficient HA (CDHA, Ca/P atom ratio between 1.33 and 1.55) was formed on the Mg substrate after HT treatment. As shown in Fig. 1g, the surface of FH-Mg was much smoother than that of HT-Mg. At $20,000\times$ magnification Fig. 1h), the surface of FH-Mg was composed of nanorod-like HA crystals. The EDS in Fig. 1i showed that the coating mainly contained the elements of Ca, P, Mg, Na, F and O. The fluorine element originated from the MgF_2 formed on the surface of Mg substrate in the process of fluoride treatment prior to the hydrothermal treatment. The average Ca/P atom ratio of FH treated specimens was calculated to be approximately 1.40, indicating the formation of CDHA on Mg substrate after FH treatment.

As shown in Fig. 2(a–b), the CDHA coating obtained by HT and FH treatment both exhibited a bi-layer structure, the inner compact layer being approximately $2\mu\text{m}$ and the outer coarse layer being approximately $1\sim 2\mu\text{m}$. Element mapping images of Ca, P, Mg, and F are also shown in Fig. 2c–f, there existed a MgF_2 layer of approximately $2\mu\text{m}$ beneath the HA layer, and no obvious interface was observed between the MgF_2 layer and the CDHA layer. 3D optical profiler images of the four groups of specimens were shown in Fig. 2(g–j). The R_a values of different specimens were 35 nm , 29 nm , 144 nm , and 32 nm , respectively, indicating that HT treatment significantly increased the surface roughness of the specimens and there were few changes of the R_a value for the Mg discs after FH treatment. As shown in Fig. 2k, the contact angle value of the as-polished Mg was $81.2 \pm 3.1^\circ$. After the different treatments, the contact angle of the HF-Mg, HT-Mg and FH-Mg

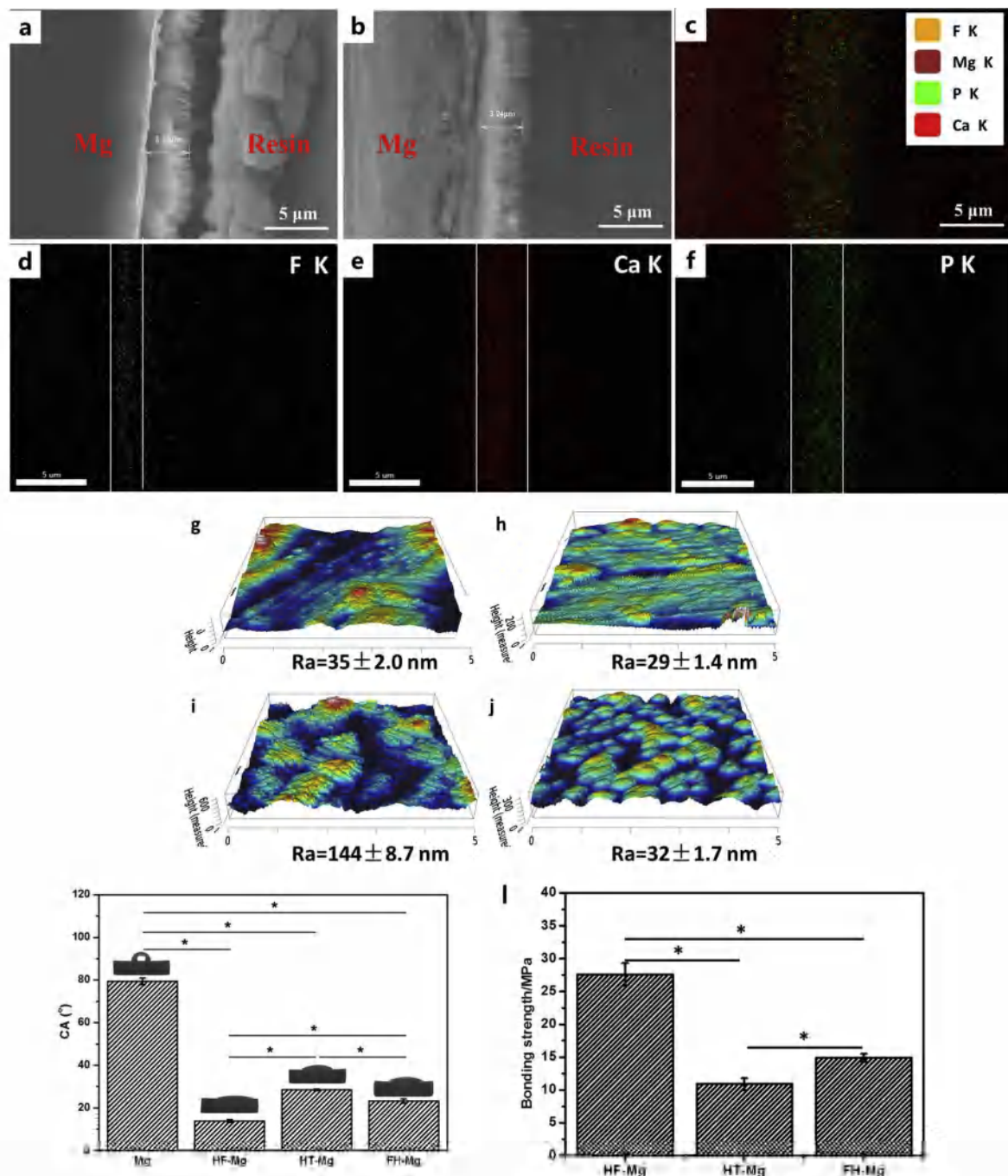


Fig. 2. SEM micrographs of the cross-section of HT-Mg (a) and FH-Mg (b); (c-f) EDS map scan results of the cross-section of FH-Mg; 3D optical profiler images of Mg (g), HF-Mg (h), HT-Mg (i), FH-Mg (j); (k) Water contact angles of Mg, HF-Mg, HT-Mg, and FH-Mg; (l) Bonding strength between different coatings and magnesium substrates, asterisks (*) indicate statistical significance, $p < 0.05$.

decreased to $14.5 \pm 1.9^\circ$, $28.5 \pm 1.7^\circ$ and $23.2 \pm 1.5^\circ$, respectively. Fig. 2l shows the measured bonding strength of different coatings on the Mg substrate. The bonding strength of the MgF₂ coating, CDHA coating, and CDHA/MgF₂ bi-layer coating with Mg substrate were 27.64 ± 1.7 MPa, 10.90 ± 0.9 MPa, and 14.93 ± 0.6 MPa, respectively.

2.2. Corrosion resistance of various coatings

Fig. 3a and 3b showed the polarization curves and the Nyquist diagrams of different specimens tested in SBF solution at 37°C. The values of the corrosion potential (E_{corr}), the corrosion current density (i_{corr}),

and the polarization resistance (R_p) are summarized in Table 1. The corrosion potentials for Mg, HF-Mg, HT-Mg and FH-Mg are -1.93 V, -1.61 V, -1.57 V and -1.45 V, respectively. The current densities of HT-Mg and FH-Mg are $4.70 \mu\text{A}/\text{cm}^2$ and $2.24 \mu\text{A}/\text{cm}^2$, which are two orders of magnitude lower than that of Mg, and one order of magnitude lower than that of HF-Mg ($22.0 \mu\text{A}/\text{cm}^2$).

In Fig. 3c, R_s is the resistance of the SBF solution. CPE_b and R_b are the capacitance and charge transfer resistance of electric double layer at the Mg/solution interface, respectively. CPE_c and R_c represent the capacitance and the resistance of the MgF₂, HA, and HA/MgF₂ bilayered coating. R_{ct} refers to the charge transfer resistance, and CPE_{dl} the electric double layer capacity. Among the four groups, FH-Mg possessed

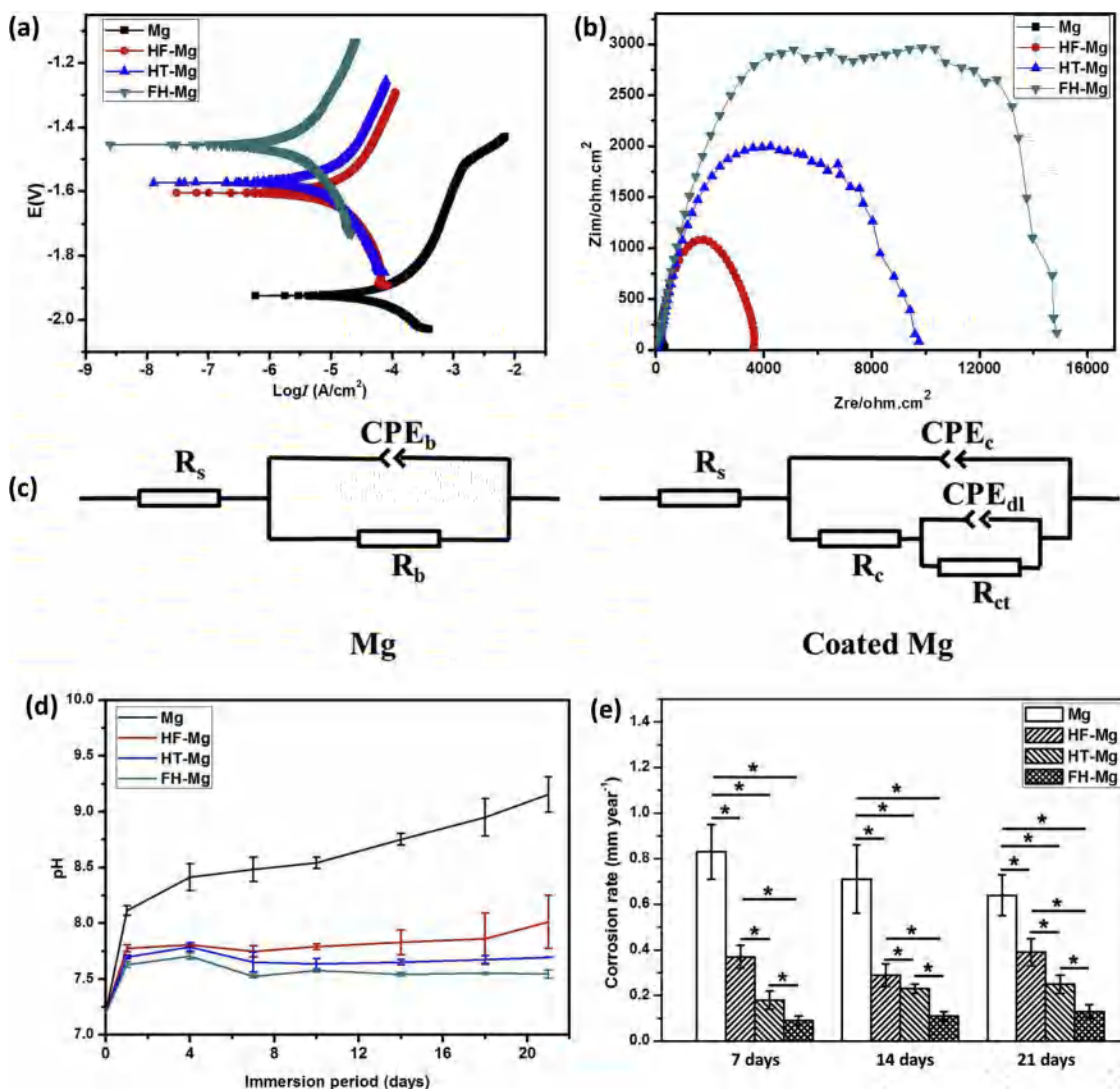


Fig. 3. Polarization curves (a) and impedance spectrum (b) of Mg, HF-Mg, HT-Mg, and FH-Mg in SBF solution; (c) equivalent circuits used to fit the impedance data of bare Mg, HF-Mg, HT-Mg, and FH-Mg discs; (d) pH variations of SBF solution immersed with Mg, HF-Mg, HT-Mg and FH-Mg as a function of the immersion time; (e) average corrosion rate for Mg, HF-Mg, HT-Mg and FH-Mg after immersion test in SBF solution for 7, 14 and 21 days, asterisks (*) indicate statistical significance, $p < 0.05$.

Table 1
Electrochemical parameters obtained from potentiodynamic polarization curves and impedance spectrum.

Specimen	Corrosion potential, E_{corr} (V)	Corrosion current density, i_{corr} ($\mu\text{A}/\text{cm}^2$)	Polarization resistance, R_p , ($\text{k}\Omega \text{cm}^2$)
Mg	-1.93	331.00	6.9
HF-Mg	-1.61	22.00	74.5
HT-Mg	-1.57	4.70	417
FH-Mg	-1.45	2.24	819

the highest corrosion resistance.

The pH variations of SBF were recorded at day 1, 4, 7, 10, 14, 18, 21 as shown in Fig. 3d. The pH values of SBF solution immersed with Mg, HF-Mg, HT-Mg and FH-Mg presented upward trend with different rates during the immersion experiment. At the first day, a significant pH increase was observed for the four groups. The pH of the SBF solutions reached 9.15, 8.01, 7.69 and 7.55 at the end of the immersion experiment for Mg, HF-Mg, HT-Mg and FH-Mg, respectively, which indicated that the coatings decreased the corrosion rate of the Mg substrate. Fig. 3e shows the corrosion rate of the four groups calculated by mass

loss after immersion for 7, 14 and 21 days in SBF solution. A trend consistent with Fig.3d was observed. Among the three coatings, the CDHA/MgF₂ bi-layer coating showed the strongest protection to the Mg substrate.

Fig. 4A shows the surface morphologies of Mg, HF-Mg, HT-Mg and FH-Mg after immersion in SBF solution at 37 °C for 7, 14 and 21 days. After immersion for 7 and 14 days, the surface of the Mg presents a cracked appearance due to the dehydration of the corrosion layer after drying. At 21 days, the surface of the Mg was completely covered by corrosion products. As for HF-Mg, only few cracks were observed on the surface of HF-Mg after immersion in SBF for 7 days, more and more cracks appeared on the surface of HF-Mg with the immersion time increased. And obvious surface damage was observed for the HF-Mg at 21 days, the surface of HF-Mg was obviously damaged. As for HT-Mg, its surface morphology did not change after immersion for 7 days. With the prolonging of immersion time, the HA coating broke into pieces at day 21. As shown in Fig.4A (j-l), no changes occurred on the surface of the FH-Mg after immersion for 7 days. While some precipitated phase particles formed on the surface at day14. Finally, the surface was completely covered by a layer of compact mineralized layer at day 21. Fig. 4B showed the surface morphologies and Ca/P ratio of HT-Mg and

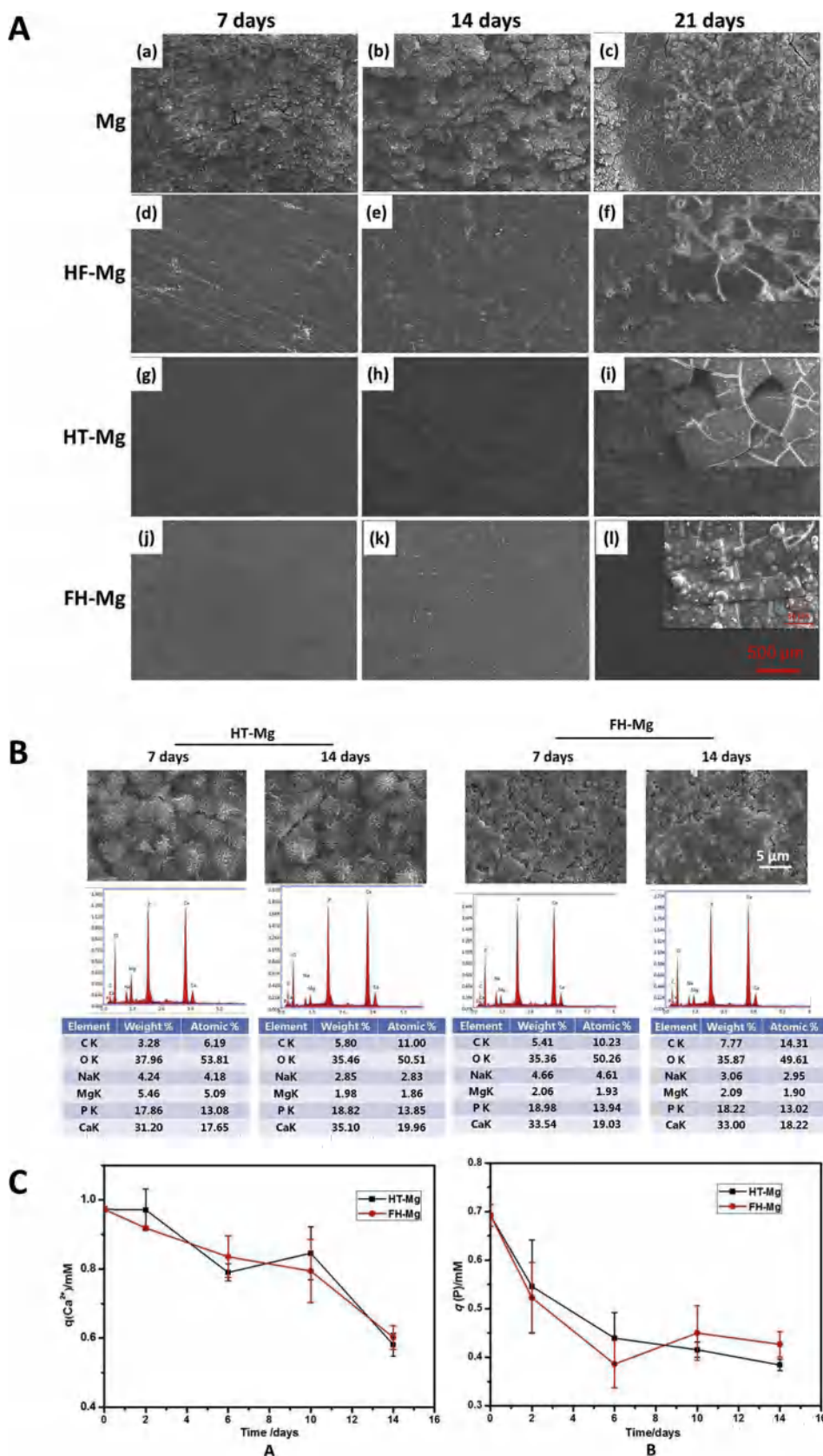


Fig. 4. A: SEM micrographs of (a-c) Mg and (d-f) HF-Mg, (g-i) HT-Mg, (j-l) FH-Mg after immersion in SBF solution for 7 days, 14 days and 21 days. B: The changes of surface morphologies and Ca/P ratio of HT-Mg and FH-Mg during immersion experiment in DMEM; C: The changes of Ca^{2+} and PO_4^{3-} concentration of the DMEM during immersion test.

HF-Mg after immersion in DMEM for 7 and 14 days. It was observed that apatite was deposited on the surfaces of HT-Mg and FH-Mg, and more and more apatite was deposited with the immersion time. The EDS results showed that the Ca/P ratio of the specimens surface was between 1.35 and 1.45 after immersion in DMEM, which was similar to that of the surface coatings before immersion. Additionally, C element was observed on the sample surface. On the one hand, element C comes from the organic components in the medium adsorbed on the specimens surface, on the other hand, the apatite layer deposited on the sample surface may be carbonated apatite layer. The concentration of calcium and phosphorus in the DMEM culture medium was detected by ICP-OES. As shown in Fig. 4C, the concentration of calcium and phosphorus in the culture medium decreased significantly at 2, 6, 10 and 14 days, which was originated from the consumption of the calcium and phosphorus from the culture medium during the deposition of the apatite layer.

2.3. Biological properties

2.3.1. In vitro Cytotoxicity and cell proliferation

CCK8 assay and live/dead staining were carried out to evaluate the proliferation of MG63 cells on the surfaces of HF-Mg, HT-Mg and FH-Mg. There were obvious differences between groups in terms of cell viability and proliferation. From Fig. 5a, it can be seen that the proliferation of MG63 cells adhered on various surfaces were in the following order: HF-Mg < HT-Mg < FH-Mg. Fig. 5b-j shows the cells survived on all the specimens, as observed by their staining patterns where no staining of dead cells (red staining) could be visualized. And it also can be seen that the cells proliferated rapidly in all groups as the culture time increased.

As shown in Fig. 6A, the initiate attachment state of MG63 cells on the surfaces of HF-Mg, HT-Mg, and FH-Mg for 1, 4 and 24 h was observed by CLSM. After 1 h, MG63 cells on the HF-Mg exhibited a roundish morphology, and a relatively spindle-shaped morphology was observed for the MG63 cells on the surfaces of HT-Mg and FH-Mg. After 4 h, more roundish cells were adhered on the HF-Mg. Cells on FH-Mg exhibited a more extended morphology compared to those on HT-Mg. After 24 h, some cells adhered on HF-Mg began to exhibit a spindle-shaped morphology. There were still few roundish cells on the surface of HT-Mg, while there existed no roundish cells observed on FH-Mg. The results indicate that FH-Mg with nanorod-like HA/MgF₂ bi-layer coating provides a more suitable surface for early cell adhesion.

The morphology of MG63 cells attached on the surfaces of HF-Mg, HT-Mg and FH-Mg for 1, 4 and 7 days were observed by SEM as shown

in Fig. 6B. After culturing for 1 day, the cells on HF-Mg did not spread well, while cells on the surface of HT-Mg and FH-Mg presented larger spreading area than those on the surface of HF-Mg, which is consistent with the results as observed by CLSM. After 4 days, more cells with polygonal morphology were observed on the surface of HT-Mg and FH-Mg. The spreading area of the cells on HT-Mg and FH-Mg was significantly larger than that of the cells on HF-Mg. Compared with HT-Mg, there were more cells grown on FH-Mg. After 7 days, MG63 cells on FH-Mg reached almost confluence. The results indicate that the MG63 cells exhibited the best spread and proliferation on Mg with nanorod-like CDHA/MgF₂ bi-layer coating.

2.3.2. Cell differentiation

Fig. 7a shows ALP activity of MG63 cells cultured on the surface of HF-Mg, HT-Mg, and FH-Mg for 7 and 14 days. At each time point, ALP activity of the cells cultured on the surface of HT-Mg and FH-Mg was much higher than that on HF-Mg, and there was no significant difference between HT-Mg and FH-Mg. After culture for 7 days and 14 days, relative Runx2 and OCN mRNA levels on FH-Mg were significantly higher than these on HF-Mg and HT-Mg. As for the expression of Col-1 and OPN at day 7, higher expression levels were observed for HT-Mg and FH-Mg than those for HF-Mg. However, there was no significant difference between HT-Mg and FH-Mg for the expression of Col-1 and OPN at day 7. At 14 days, FH-Mg exhibited significantly higher relative mRNA expression levels of Col-1 and OPN.

3. Discussion

In this study, we fabricated a CDHA/MgF₂ bilayer coating with nanorod-like morphology on Mg by the combination of fluoride treatment and hydrothermal treatment. In comparison with CDHA coating, the CDHA/MgF₂ bi-layer coating presented a smoother surface with nanorod-like morphology. The surface roughness of CDHA/MgF₂ bi-layer coating is basically consistent with that of the Mg substrate before treatment, which is much lower than that of the CDHA coating prepared directly by hydrothermal treatment. The different surface topography results from different surface states of Mg and HF-Mg before hydrothermal treatment. Correia et al. reported that Mg²⁺ ions could change the morphology of the HA coating by inhibiting the growth rate of the crystals [14]. When Mg discs without fluoride treatment were placed in the hydrothermal reaction solution, pit corrosion firstly occurred on the surface of Mg substrate with the following reaction:

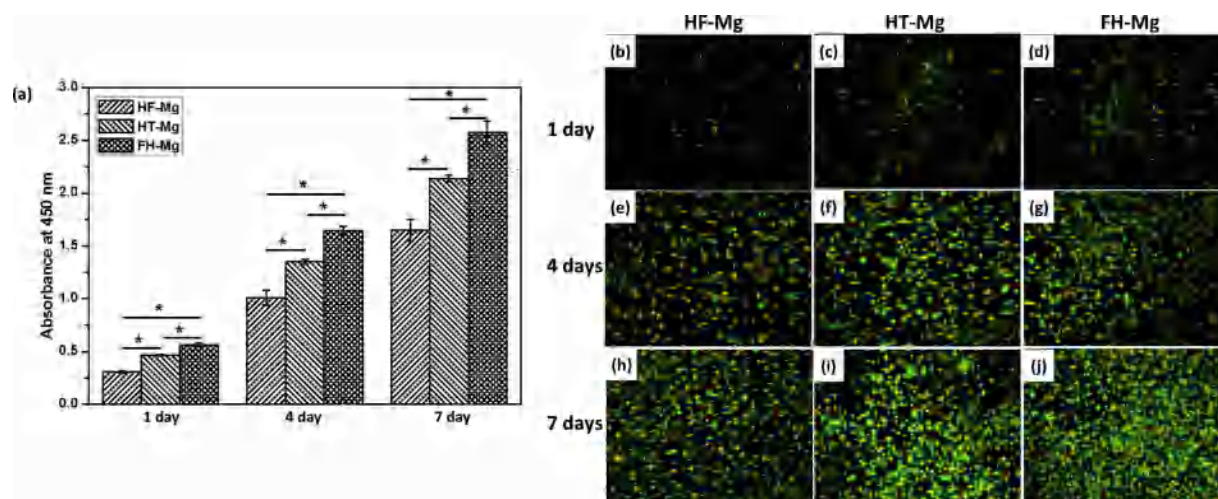
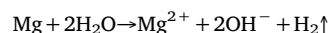


Fig. 5. (a) Measurement of MG63 cells proliferation by CCK-8 assay after 1, 4, and 7 days incubation. For each group, n = 3; asterisks (*) indicate statistical significance, p < 0.05; live-dead staining of MG63 cells cultured on the surface of HF-Mg (b, e, h), HT-Mg (c, f, i), and FH-Mg (d, g, j) at day 1, 4, and 7.

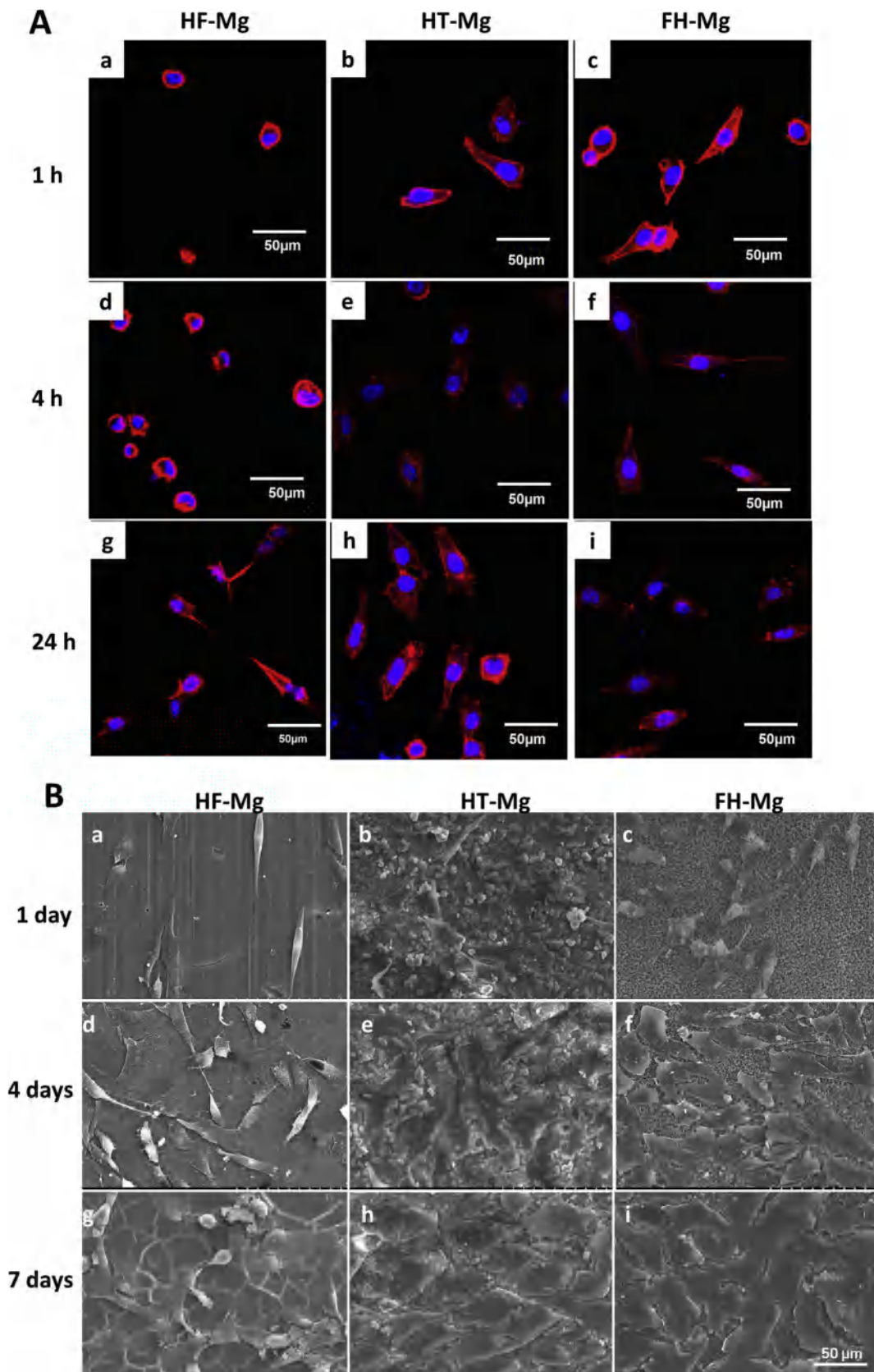


Fig. 6. A: Actin (red) and cell nucleus (blue) fluorescence images of MG63 cells cultured on the surfaces of HF-Mg (a, d, g), HT-Mg (b, e, h), and FH-Mg (c, f, i) for 1, 4 and 24 h; (For interpretation of the references to colour in this figure legend, the reader is referred to the web version of this article).

B: SEM micrographs of the MG63 cells adhered on the surfaces of HF-Mg (a, d, g), HT-Mg (b, e, h) and FH-Mg (c, f, i) after culturing for 1, 4 and 7 days.

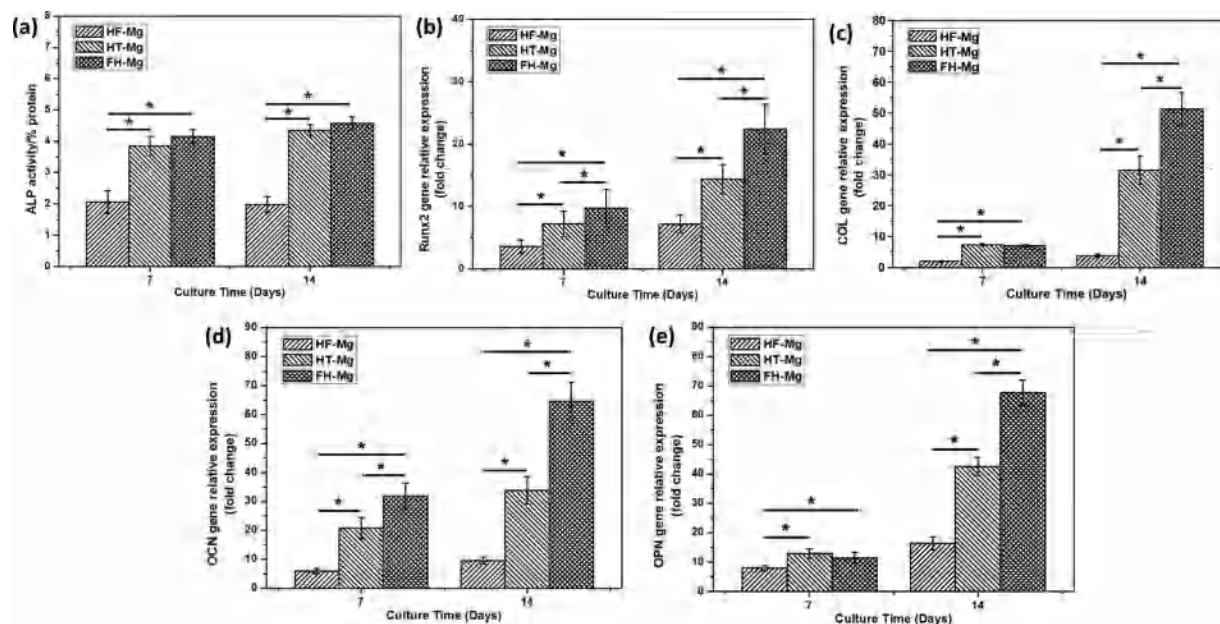


Fig. 7. (a) The ALP activity of MG63 cells cultured on the surfaces of HF-Mg, HT-Mg and FH-Mg for 7 and 14 days. The value of ALP activity was normalized to the total protein level of the specimens; relative mRNA levels of main osteogenic differentiation markers on HF-Mg, HT-Mg and FH-Mg: (b) Runx2; (c) Col-I; (d) OCN; (e) OPN, * $p < 0.05$ between test group.

The reaction resulted in the increase of local Mg^{2+} concentration, which inhibited the growth of CDHA. Therefore, heterogeneous nucleation and crystal growth took place on the surface of bare Mg discs during the hydrothermal reaction. Since the location of pit corrosion is non uniform, the growth of CDHA coating on the surface of magnesium is also non uniform, thus leading to higher roughness of the CDHA coating obtained on the surface of Mg substrate. As for the FH-Mg, a passivated MgF_2 layer was firstly obtained on the surface of Mg substrate. The MgF_2 layer is stable in the hydrothermal reaction solution, and homogeneous nucleation and growth of CDHA coating could be achieved on the surface of the MgF_2 layer. So surface roughness of the CDHA/ MgF_2 bi-layer coating was not increased by the hydrothermal treatment. Generally, the surface with roughness less than 100 nm is considered as nano-topography, and 100 nm ~ 1 μ m as submicron surface topography [15]. In this study, the CDHA/ MgF_2 bi-layer coating presented nano-scale surface morphology, while the CDHA coating presented submicron scale surface topological morphology. Surface topography has been demonstrated to have significant impact on the behaviors of osteoblasts [16]. To improve the adhesion, proliferation and differentiation of osteoblasts on the implant surface by optimizing the topological structure of the implant surface is an important method to enhance the biological performance of the implant. Yang et al. compared the influences of different surface topographies on osteoblast morphology. It was found that cells spread well and exhibited typical squamous shape on nano-scale surface, whereas they became more elongated and polarized on submicron scale and micrometer-scale surface [17].

Adhesion test results showed that MgF_2 interlayer enhanced the bonding strength between the CDHA coating and the Mg substrate. This finding is consistent with the result as reported by Ren et al., they used MgF_2 as an interlayer between CaP bioglass coating and the Mg substrate, significantly enhance bonding strength between the bioglass coating and Mg substrate was observed [18]. The main reason is that the existence of the MgF_2 interlayer weakened the mismatch of the hardness and thermal expansion coefficient between the HA coating and the Mg substrate, which led to decreased residual stress between the HA coating and the Mg substrate, thus increasing the bonding strength. High bonding strength is expected to lower the risk of the coating falling off in the using process, which is beneficial to avoid the

occurring of rapid local corrosion, thus keeping the mechanical integrity of Mg-based implants.

The specimens after the surface modification have more positive corrosion potentials, lower corrosion current densities and larger polarization resistances. FH-Mg presented the highest corrosion potential and the lowest current density. In vitro immersion test results showed that a rapid increase in pH value was observed for the four groups at the first day of the immersion experiment. FH-Mg presented the minimal pH value increase of the SBF, which had been below 7.75. It can be expected that bone absorption caused by local high pH can be to a great extent inhibited by the CDHA/ MgF_2 bi-layer coating. The corrosion of HA coated Mg started from the damaged part of the coating in the immersion process, and the immersion solution attacked the Mg substrate from the damaged part of the coating, causing the degradation of Mg. The improvement of the corrosion resistance of FH-Mg comes, on the one hand, from the higher bonding strength between CDHA coating and MgF_2 coating. That is because the top layer of CDHA coating was not easy to be damaged during the immersion experiment. On the other hand, even if the CDHA coating is partially damaged, the presence of the dense MgF_2 intermediate layer further isolated the contact between SBF and the Mg substrate, thus delaying the degradation of Mg. In addition, it can be seen that apatite particle deposited on the surface of the FH-Mg at day 14. At day 21, dense apatite mineralized layer formed on the surface of CDHA/ MgF_2 bi-layer coating. The existence of dense mineralized layer further isolated Mg substrate from the immersion solution, improved the corrosion resistance of Mg, therefore, the CDHA/ MgF_2 bi-layer coating is expected to provide a long term protection to the Mg substrate.

The biological properties of biomaterials are closely related to the ionic interactions between the materials and the surrounding media [19]. In this study, the exchange of calcium ions and phosphate ions between CDHA coating and DMEM medium was characterized by immersion experiment. The result showed that apatite layer deposited on the surface of CDHA coating and calcium ions and phosphate ions in the DMEM decreased with the immersion time. This result is not consistent with that reported by Gustavsson et al. [20]. They have reported that HA uptaked calcium ion and release phosphate ions from the medium. The reason for this phenomenon may be owing to the different morphologies between the CDHA coating of this study and the CDHA

samples as reported in the study of Gustavsson et al. In this research, CDHA coating is in the shape of nanoneedle or nanorod, while in Gustavsson et al., the surface of the CDHA sample is in the shape of plate. Theoretically, the specific surface area of CDHA coating in this study is larger and the surface energy is higher, so it is more conducive to the adsorption of protein in the culture medium and the nucleation and deposition of apatite on the surface of the coating, resulting in the consumption of calcium and phosphorus elements in the DMEM culture medium. According to the deposition of apatite layer, during the cell experiment, the medium near the CDHA coating had high concentration of calcium ions and phosphate ions, which was supposed to promote the osteogenic differentiation of MG63 cells.

Significantly enhanced adhesion, proliferation and differentiation of MG63 cells was observed on FH group with nanorod-like CDHA/MgF₂ bi-layer coating, besides the chemical component of the bi-layer coating, its nano-scale surface morphology also plays an important role. It was reported that surface roughness smaller than 100 nm appeared to promote protein adsorption better than features larger than 100 nm [21]. Webster et al. investigated functions of osteoblasts on nanophase ceramics and provided confirmed evidence of enhanced osteoblast proliferation and differentiation on nanophase ceramics than on conventional ceramics [22]. The nanoscale surface structure is similar to the microstructure of natural extracellular matrix, which is recognized as an important factor for the osteoblast adhesion, proliferation and differentiation [23]. The nanoscale surface morphology is beneficial of the adsorption of vitronectin, which possesses relatively small and linear molecule (15 nm in length) [24]. There are strong affinity between vitronectin and osteoblasts. Vitronectin is preferentially recognized by osteoblasts, so it has been proven that the nanoscale surface morphology is especially conducive to the osteoblast adhesion on its surface [25]. Pang et al. fabricated rod-like and flake-like HA coating on Mg by electrodeposition method. They found that the rod-like HA coating is more beneficial to the spreading, proliferation and differentiation of MC3T3-E1 cells [5]. They speculated that ordered assembly structure of the HA might cause topography-dependent coordination with biomolecules for enhancing osteoblast-like cell proliferation and osteogenic differentiation. Therefore, it can be confirmed that CDHA coating with nanoscaled surface morphology is beneficial to the enhanced bioactivity associated with osteogenesis of Mg. From these results, it can be hypothesized that the nanorod-like CDHA/MgF₂ bi-layer coating would help to improve osseointegration of Mg-based implants by promoting new bone formation on implant surface, thus shortening contact time between Mg and the surrounding body fluid and reducing the degradation rate of Mg-based implants in vivo. Next, we will study the degradation behavior and osteogenetic bioactivity of Mg-based orthopedics implants with CDHA/MgF₂ bi-layer coating in vivo.

4. Conclusion

In this study, we fabricated a CDHA/MgF₂ bi-layer coating on Mg using a combination of fluoride treatment and hydrothermal treatment. The CDHA/MgF₂ bi-layer coating possesses nano-scale roughness, strong adhesion strength with Mg substrate. Immersion test and electrochemical test indicated that the corrosion resistance of Mg was significantly improved by the CDHA/MgF₂ bi-layer coating, which offered favorable long-term protection for Mg substrate. In vitro studies demonstrated that the HA/MgF₂ bi-layer coating enhanced the attachment, proliferation and differentiation of MG63 cells. This work provides a promising method for the surface modification of Mg-based bone implants with appropriate degradation rate and bioactivity associated with osteogenesis.

CRedit authorship contribution statement

Junlei Li: Conceptualization, Methodology, Writing - original draft, Funding acquisition. **Wenwu Xu:** Validation, Investigation, Data

curation. **Xiao Lin:** Writing - review & editing, Methodology. **Fang Cao:** Methodology, Validation. **Jiahui Yang:** Methodology. **Lu Li:** Formal analysis. **Xiaowei Wei:** Methodology. **Xiuzhi Zhang:** Methodology. **Dewei Zhao:** Conceptualization, Supervision, Project administration, Funding acquisition. **Ke Yang:** Writing - review & editing, Methodology.

Declaration of Competing Interest

No conflict of interest exists in the submission of this manuscript, and manuscript is approved by all authors for publication. I would like to declare on behalf of my co-authors that the work described was original research that has not been published previously, and not under consideration for publication elsewhere, in whole or in part.

Acknowledgement

This work was supported by the National Key R&D Program of China (Grant No. 2016YFC1102000), National Natural Science Foundation of China (Grant No. 81672139 and 81702129), Doctor Initial Foundation of Liaoning Province (No. 20170520017) and Affiliated Zhongshan Hospital of Dalian University (No. DLDXZSY-DK201701).

Appendix A. Supplementary data

Supplementary material related to this article can be found, in the online version, at doi:<https://doi.org/10.1016/j.colsurfb.2020.110911>.

Experimental section; preparation and characterization of specimens; used characterization methods; methods and procedures of cell experiments; statistical analysis method.

References

- [1] M.P. Staiger, A.M. Pietak, J. Huadmai, G. Dias, Magnesium and its alloys as orthopedic biomaterials: a review, *Biomaterials* 27 (2006) 1728–1734.
- [2] S.V. Dorozhkin, Calcium orthophosphate coatings on magnesium and its biodegradable alloys, *Acta Biomater.* 10 (2014) 2919–2934.
- [3] S. Shadanbaz, G.J. Dias, Calcium phosphate coatings on magnesium alloys for biomedical applications: a review, *Acta Biomater.* 8 (2012) 20–30.
- [4] X. Lin, L. Tan, Q. Wang, G. Zhang, B. Zhang, K. Yang, In vivo degradation and tissue compatibility of ZK60 magnesium alloy with micro-arc oxidation coating in a transcortical model, *Mater. Sci. Eng. C Mater. Biol. Appl.* 33 (2013) 3881–3888.
- [5] S. Pang, Y. He, P. He, X. Luo, Z. Guo, H. Li, Fabrication of two distinct hydroxyapatite coatings and their effects on MC3T3-E1 cell behavior, *Colloids Surf. B Biointerfaces* 171 (2018) 40–48.
- [6] Y. Song, S. Zhang, J. Li, C. Zhao, X. Zhang, Electrodeposition of Ca-P coatings on biodegradable Mg alloy: in vitro biomineralization behavior, *Acta Biomater.* 6 (2010) 1736–1742.
- [7] T. Yan, L. Tan, D. Xiong, X. Liu, B. Zhang, K. Yang, Fluoride treatment and in vitro corrosion behavior of an AZ31B magnesium alloy, *Mater. Sci. Eng. C* 30 (2010) 740–748.
- [8] J. Waterman, A. Pietak, N. Birbilis, T. Woodfield, G. Dias, M.P. Staiger, Corrosion resistance of biomimetic calcium phosphate coatings on magnesium due to varying pretreatment time, *Mater. Sci. Eng. B* 176 (2011) 1756–1760.
- [9] L.-Y. Li, L.-Y. Cui, R.-C. Zeng, S.-Q. Li, X.-B. Chen, Y. Zheng, M.B. Kannan, Advances in functionalized polymer coatings on biodegradable magnesium alloys - A review, *Acta Biomater.* (2018).
- [10] X. Liu, Z. Zhen, J. Liu, T. Xi, Y. Zheng, S. Guan, Y. Zheng, Y. Cheng, Multifunctional MgF₂/Polydopamine coating on Mg alloy for vascular stent application, *J. Mater. Sci. Technol.* 31 (2015) 733–743.
- [11] H. Wang, S. Guan, Y. Wang, H. Liu, H. Wang, L. Wang, C. Ren, S. Zhu, K. Chen, In vivo degradation behavior of Ca-deficient hydroxyapatite coated Mg-Zn-Ca alloy for bone implant application, *Colloids Surf. B Biointerfaces* 88 (2011) 254–259.
- [12] S.M. Kim, J.H. Jo, S.M. Lee, M.H. Kang, H.E. Kim, Y. Estrin, J.H. Lee, J.W. Lee, Hydroxyapatite-coated magnesium implants with improved in vitro and in vivo biocorrosion, biocompatibility, and bone response, *J. Biomed. Mater. Res. A* 102 (2014) 429–441.
- [13] S. Shadanbaz, G.J. Dias, Calcium phosphate coatings on magnesium alloys for biomedical applications: a review, *Acta Biomater.* 8 (2012) 20–30.
- [14] M.B. Correia, J.P.G. Júnior, M.C.S.S. Macedo, C.X. Resende, E.A. dos Santos, Effect of Mg 2+ on acidic calcium phosphate phases grown by electrodeposition, *J. Cryst. Growth* 475 (2017) 328–333.
- [15] L. Bacakova, E. Filova, M. Parizek, T. Ruml, V. Svorcik, Modulation of cell adhesion, proliferation and differentiation on materials designed for body implants,

- Biotechnol. Adv. 29 (2011) 739–767.
- [16] X. Liu, P.K. Chu, C. Ding, Surface nano-functionalization of biomaterials, *Mater. Sci. Eng. R Rep.* 70 (2010) 275–302.
- [17] L. Yang, Z. Gong, Y. Lin, V. Chinthapenta, Q. Li, T.J. Webster, B.W. Sheldon, Disordered topography mediates filopodial extension and morphology of cells on stiff materials, *Adv. Funct. Mater.* (2017) 1702689.
- [18] M. Ren, S. Cai, T. Liu, K. Huang, X. Wang, H. Zhao, S. Niu, R. Zhang, X. Wu, Calcium phosphate glass/MgF₂ double layered composite coating for improving the corrosion resistance of magnesium alloy, *J. Alloys. Compd.* 591 (2014) 34–40.
- [19] Y.R. Shih, Y. Hwang, A. Phadke, H. Kang, N.S. Hwang, E.J. Caro, S. Nguyen, M. Siu, E.A. Theodorakis, N.C. Gianneschi, K.S. Vecchio, S. Chien, O.K. Lee, S. Varghese, Calcium phosphate-bearing matrices induce osteogenic differentiation of stem cells through adenosine signaling, *Proc Natl Acad Sci U S A* 111 (3) (2014) 990–995.
- [20] J. Gustavsson, M.P. Ginebra, E. Engel, J. Planell, Ion reactivity of calcium-deficient hydroxyapatite in standard cell culture media, *Acta Biomater.* 7 (2011) 4242–4252.
- [21] S. Samavedi, A.R. Whittington, A.S. Goldstein, Calcium phosphate ceramics in bone tissue engineering: a review of properties and their influence on cell behavior, *Acta Biomater.* 9 (2013) 8037–8045.
- [22] T.J. Webster, C. Ergun, R.H. Doremus, R.W. Siegel, R.J.B. Bizios, Enhanced functions of osteoblasts on nanophase ceramics, *Biomaterials* 21 (2000) 1803–1810.
- [23] R.L. Price, K. Ellison, K.M. Haberstroh, T.J. Webster, Nanometer surface roughness increases select osteoblast adhesion on carbon nanofiber compacts, *J. Biomed. Mater. Res. A* 70 (2004) 129–138.
- [24] R.L. Price, M.C. Waid, K.M. Haberstroh, T.J. Webster, Selective bone cell adhesion on formulations containing carbon nanofibers, *Biomaterials* 24 (2003) 1877–1887.
- [25] K.C. Dee, T.T. Andersen, R.J. Bizios, Design and function of novel osteoblast-adhesive peptides for chemical modification of biomaterials, *J. Biomed. Mater. Res.* 40 (1998) 371–377.